

Article

Experimental Study of Dimensional Effects on Tensile Strength of GFRP Bars

Hongbo Liu ¹, Thierno Aliou Ka ^{2,*} , Nianjiu Su ¹, Yaoyu Zhu ³, Shuai Guan ⁴, Jinxi Long ⁴ and T. Tafsirojjaman ⁵ 

¹ Poly Changda Engineering Co., Ltd., No. 942, Middle Guangzhou Avenue, Tianhe District, Guangzhou 510620, China; lhb2023001@163.com (H.L.); nianjiusu@126.com (N.S.)

² Research Institute of Urbanization and Urban Safety, School of Civil and Resource Engineering, University of Science and Technology Beijing, 30 Xueyuan Road, Beijing 100083, China

³ CCCC Highway Bridges National Engineering Research Center Co., Ltd., No. 23, Huangsi Street, Xicheng District, Beijing 100120, China; zhuyaoyu@bnerc.com

⁴ The Key Laboratory of Urban Security and Disaster Engineering of Ministry of Education, Beijing University of Technology, Pingleyuan Road 100, Beijing 100124, China; guuwalgia1906@gmail.com (S.G.); longjinxi@emails.bjut.edu.cn (J.L.)

⁵ School of Architecture and Civil Engineering, The University of Adelaide, Adelaide 5005, Australia; tafsirojjaman@adelaide.edu.au

* Correspondence: d202361002@xs.ustb.edu.cn

Abstract: This study explores the mechanical properties of Glass Fiber-Reinforced Polymer (GFRP), a high-performance composite material, focusing on how varying diameters affect its tensile strength, modulus, and elongation. Experimental data obtained from three sets of tensile tests on 10, 12, and 25 mm bars helped establish a stress–strain relationship for GFRP reinforcements, considering diameter changes, and a formula for calculating the ultimate tensile strength based on diameter. Utilizing the weakest chain theory and the Weibull distribution, the research found that GFRP’s tensile strength diminished with increased diameter, while the elastic modulus behaves oppositely. The analysis, grounded in the weakest chain theory, identifies the specimen’s effective volume as a critical factor in the size effect of GFRP bars. Moreover, the study proves a significant size effect on GFRP’s tensile properties, validating the theory’s application in predicting the strength of GFRP bars of varying sizes and recommending a specimen length range of 30–40 times its diameter for standardization purposes.

Keywords: glass fiber-reinforced plastics; tensile testing; mechanical properties; size effect; weakest chain theory; Weibull distribution



Citation: Liu, H.; Ka, T.A.; Su, N.; Zhu, Y.; Guan, S.; Long, J.; Tafsirojjaman, T. Experimental Study of Dimensional Effects on Tensile Strength of GFRP Bars. *Buildings* **2024**, *14*, 1205. <https://doi.org/10.3390/buildings14051205>

Academic Editor: Dan Bompa

Received: 21 March 2024

Revised: 17 April 2024

Accepted: 20 April 2024

Published: 24 April 2024



Copyright: © 2024 by the authors. Licensee MDPI, Basel, Switzerland. This article is an open access article distributed under the terms and conditions of the Creative Commons Attribution (CC BY) license (<https://creativecommons.org/licenses/by/4.0/>).

1. Introduction

GFRP is an innovative composite material made from resin and glass fiber. It offers several superior properties, including high specific strength, excellent impact resistance, corrosion resistance, and non-magnetic properties. The use of GFRP reinforcement as a replacement for conventional steel reinforcement in concrete structures has been widely proven to be an effective method, especially in solving the problem of corrosion of steel reinforcement. GFRP reinforcement has been successfully used in a variety of applications such as bridges, hydraulic structures, port terminals, temporary reinforcement of coal mines, and permanent slope reinforcement works. Its excellent performance has resulted in reliable reinforcement and strengthening of these projects while supporting the long-term stability and sustainability of the structures [1–3].

Many important results have been obtained on the mechanical properties and engineering applications of FRP reinforcement. In the quasi-static study of FRP reinforcement, some scholars have proposed a new approach by suggesting the embedding of tailor-made conical anchors at both ends of the reinforcement. The purpose of this method is to prevent the sliding phenomenon during the tensile strength test, thus ensuring the accuracy and

reliability of the experiment. Using this specially designed tapered anchor method enhances the performance of GFRP reinforcement in engineering tasks, leading to increased stability and durability of the structure [4,5]. A uniquely designed anchor plays a crucial role in addressing bond failures effectively. ACI 440 recommends a gauge length of $40d$ (d being the diameter of the GFRP) for FRP reinforcement in tensile tests [6]. Li et al. [7] found that the tensile strength and elongation of GFRP tendons increased significantly with increasing loading rate, mainly due to the specific rate-dependent viscoelastic properties of epoxy polymers. FRP reinforcement is temperature sensitive [8,9]. The tensile strength of FRP reinforcement decreases with increasing temperature. The GFRP reinforcement loses its tensile strength when the temperature reaches $450\text{ }^{\circ}\text{C}$. The residual tensile strength and modulus of the GFRP reinforcement decrease with increasing temperature [10]. The influence of FRP bar characteristics on their performance is also noteworthy. For instance, the mechanical properties, particularly the tensile strength, of FRP bars are significantly influenced by the fiber-to-matrix ratio. However, it should be noted that this ratio might not always be the decisive factor in determining performance under elevated temperatures. Instead, factors such as the bar's diameter, type of fiber, type of resin, and thermal properties play a more consequential role [11]. On the other hand, the effects of seawater or alkaline environments on GFRP tendons have been investigated [12,13], and damage prediction models have been developed. Ahmed et al. reviewed the durability of FRP seawater sea sand concrete (FRP-SWSSC) and indicated that the saline/alkaline environment is a major threat to the long-term performance of GFRP reinforcement of FRP-SWSSC [14]. Although many studies have been conducted on the mechanical properties of FRP tendons in the quasi-static state, the size effect is also an essential characteristic of quasi-brittle material [15,16] that needs special attention. However, the study of the dimensional effects of FRP tendons is limited [17]. For GFRP bars, the size effect is mainly manifested in the decrease in strength with the increase in member size, which is very different from that of steel bars and has attracted the attention of the engineering community. Considering the relatively recent development of GFRP bars' research and application, there are few studies on the size effect, which are mainly limited to the fitting of experimental results, and there is a lack of theoretical analyses [18,19].

GFRP bars of different diameters are tested for their strength and other mechanical properties during design. Nevertheless, due to the strong size effect, the results of different test methods may differ greatly from the actual application. For example, a unified understanding of the relationship between the length and diameter of the specimen has not yet been formed [20]. Domestic and international standards for tensile testing of GFRP bars are few and unrecognized. In order to better promote the application of FRP bars in civil engineering, a detailed study of the size effect on the mechanical properties of GFRP bars is necessary and will provide a basis for the design of GFRP bars. In this paper, the tensile mechanical properties of GFRP bars with different diameters are investigated in terms of their dimensional effects through experiments. Moreover, an analytical model was developed to predict the tensile strength of GFRP tendons based on the weakest chain theory. Detailed explanations of the model development and the use of the weakest chain theory are provided in the theoretical basis section of this paper.

2. Review on the Size Effect of FRP Bars

Numerous studies have documented the significant influence of FRP laminate layer on its strength performance. For instance, Hossein et al. [21] conducted a study on the static capacity of tubular X-joints reinforced with FRP, revealing that an increase in the number of FRP layers enhances the overall performance of the joints. This improvement is manifested by a reduction in the deformation and an increase in the equivalent plastic strain in joints that are reinforced with a greater number and thickness of FRP layers.

However, it is worth noting that the research on the size effect of GFRP bars specifically examining the impact of bar diameter on its strength properties remains limited in scope. Further investigation in this area is needed to gain a thorough understanding of how the diameter of GFRP bars influences their strength performance.

Lee et al. [22] explored the bond behavior of GFRP bars in high-strength concrete, particularly the effect of bar diameter. Their findings indicate a significant reduction in bond strength with increasing bar thickness, a trend more pronounced in GFRP than in steel. This study contributes to the understanding of how GFRP bars interact with concrete of different strengths but calls for more research on optimizing bond performance for larger diameters. Research studies have also indicated that the bond performance of FRP bars in seawater sea-sand concrete (SSC) is adversely influenced by larger diameters and bond lengths. According to Li. Sun et al. [23], the bond strength between FRP bar and sea sand coral concrete (SSCC) diminishes as the diameter and bond length of the bar increases. However, an increase in the strength grade of SSCC has been shown to improve the bond strength of the bar. Similar observations were made in the case of SSC with geopolymer binders. In fact, the latter demonstrated a notable improvement in the bond behavior of FRP bars, particularly in terms of bond rigidity, resulting in an approximate three times increase in initial bond stiffness [24].

In their study on the size effect in flexural behavior of unidirectional GFRP composites under bending load, Demiral et al. [25] demonstrated that specimen geometry significantly influences mechanical behavior and failure mechanisms. While providing valuable insights into designing structures with composite materials, the research highlights the need for further exploration of size-dependent performance in practical applications. However, the study calls for a more detailed investigation into the long-term performance of deformed GFRP bars in concrete structures. Al Ajarmeh et al. [26] introduced a novel testing method to characterize the compressive properties of high-modulus GFRP bar diameter and unbraced length-to-diameter ratio. They found that larger diameters and higher ratios decrease compressive strength, indicating micro-fiber buckling as a critical factor. This study opens the door for developing standard test methods for GFRP bars in compression, addressing a significant research gap. In the same vein, Xiao-hui et al. [27] conducted an experimental study on the size effect in tensile mechanical properties of GFRP rebar, applying the weakest chain theory to analyze the phenomenon. The research confirms that the size significantly affects the ultimate tensile strength, modulus of elasticity, and elongation percentage, providing a basis for calculating the ultimate tensile strength of GFRP rebars of different diameters. The study points to a clear size effect in GFRP rebars but suggests further research to standardize the effective lengths of testing specimens.

On the other hand, other researchers explored the performance of GFRP bars under various conditions, especially focusing on the structural implications of using bars of different sizes in concrete structures. Abdelkarim et al. [28] examined the flexural strength and serviceability of concrete beams reinforced with deformed GFRP bars. Their work examines the influence of different bar diameters on the overall performance of concrete beams. The study revealed that increasing the GFRP reinforcement ratios significantly affects the service moment more than the resistance moment, suggesting that deformed GFRP bars can enhance serviceability and strength. The variation in bar sizes and the reinforcement ratio could highlight the size-dependent behavior of GFRP bars, reflecting their strength and efficiency as reinforcement materials. Zinkaah et al. [29] presented an experimental study on the load capacity of continuous concrete deep beam reinforced with GFRP bars, focusing on shear span-to-depth ratio, web reinforcement, and size effect. The study contributes to understanding the size effect GFRP bars through the lens of shear strength and structural integrity of deep beam. The impact of bar diameter could reveal critical insights into how the size and placement of the GFRP bars affects the load-carrying capacity of concrete structures, hence providing a direct link to bars' strength characteristics.

From the aforementioned studies, it is clear that there is a necessity for more focused research on the size effect of GFRP bars on their tensile strength and for the development

of sophisticated prediction models that can accurately forecast the performance of GFRP reinforcement bars. Such advancements would significantly contribute to the optimization of GFRP bars for construction applications, ensuring both the structural integrity and longevity of concrete infrastructures.

3. Theoretical Basis

Statistical strength theory or statistical weakest chain theory has been the basis of traditional brittle fracture research for many years. The concept of the weakest chain was proposed by Pierce, and the weakest chain model is described in Equation (1) [30]. The weakest chain theory assumes that the material is made up of many small units and is considered to be destroyed if any unit or chain in the material fails. The probability of failure of each chain stress from 0 to σ can be described by the distribution function $F(\sigma)$:

$$F(\sigma) = 1 - \exp(-\varphi(\sigma)) \quad (1)$$

Weibull (1939) came to the crucial conclusion that a tail distribution of very low intensity with very low probability could not be described by any of the existing distributions, which came to be known in statistics as the Weibull distribution [30–32]:

$$\varphi(\sigma) = \left(\frac{\sigma - \sigma_u}{\sigma_0} \right)^m \quad (2)$$

$$Fv(\sigma) = 1 - \exp \left[-V \left(\frac{\sigma}{\sigma_0} \right)^m \right] \quad (3)$$

where σ_u is the threshold stress below which no damage occurs; V is the volume of the bar; σ_0 and m are the scale parameter and shape parameter, respectively.

The probability of damage of the sample is derived by considering each small unit volume within the sample volume as a 'chain'. To facilitate the description of the experimental data, Equation (3) has been rearranged by taking two logarithms and expressed in linear form as:

$$\ln \left[\ln \left(\frac{1}{1 - Fv(\sigma)} \right) \right] = m(\ln \sigma - \ln \sigma_0) + \ln V \quad (4)$$

σ_0 and m can be obtained by analyzing experimental data. For a material with a known volume, if its strength change can be described by Weibull distribution, the right end of Equation (4) can be drawn as a straight line, where m is the slope of the straight line and $\ln V$ is the intersection point of the straight line and the y-axis.

When the material strength conforms to the Weibull distribution, there is a correlation between the strength of the specimen or component and its size. Assuming that the scale parameter σ_0 and the shape parameter m are material constants that are independent of the specimen size and stress state, applying Formula (4) for two specimens with the same failure probability and the same stress distribution yields the following relationship:

$$\frac{\sigma_2}{\sigma_1} = \left(\frac{V_1}{V_2} \right)^{\frac{1}{m}} \quad (5)$$

Equation (5) directly links strength and material volume, allowing size effects to be quantified. The logarithm of stress and volume has a linear relationship, and the slope is equal to $-1/m$, see Figure 1.

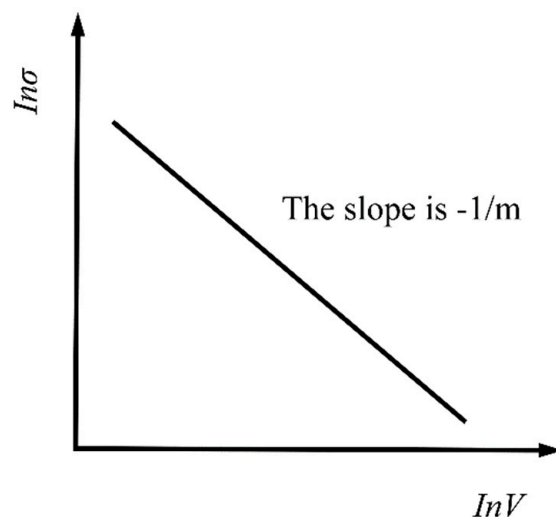


Figure 1. Intensity size effect logarithm.

4. Experimental Protocol

The purpose of the experiment in this paper is to test the mechanical properties such as ultimate tensile strength, elastic modulus, and ultimate elongation of GFRP bars at room temperature, so as to obtain the change law of GFRP bars with different diameters.

4.1. Experimental Material

The GFRP bar is a pultruded GFRP bar produced by the Shenzhen Haichuan New Material Technology Co., Ltd. Company (Shenzhen, China). The fiber used in the bar is alkali-free glass fiber, the matrix is unsaturated resin, and the fiber content is 78%. It is full-thread medium-strength glass fiber-reinforced plastic ribs. The diameters of GFRP bars used in the test are 10, 12, and 25 mm, and the manufacturing process and control measures are the same.

The adhesive is a two-component cold-curing thixotropic epoxy resin adhesive, which has high strength, good adhesion to most materials, strong waterproof and chemical corrosion resistance, and low shrinkage. It is often used in the reinforcement of concrete structures.

The specification of the steel pipe is selected according to the diameter of the GFRP tendon. The inner diameter is required to be 3–6 mm larger than the diameter, and the wall thickness should not be less than 2.5 mm.

4.2. Test Equipment

The test loading equipment is an MTS100 electro-hydraulic servo static and dynamic universal testing machine, as shown in Figure 2.

The acquisition system comprises the MTS experimental setup and a computer-based strain measurement apparatus, utilizing the TS 3890 static strain measurement processor for data collection. Axial tension in the specimen is accurately determined using an NCS-YYU-10/200 electronic extensometer. This device, built on a simply supported beam design and leveraging resistance strain principles, features a gauge length of 200 mm. It is capable of measuring deformations up to 10 mm with a minimal error margin of 0.104%, ensuring precise and reliable data for analysis.

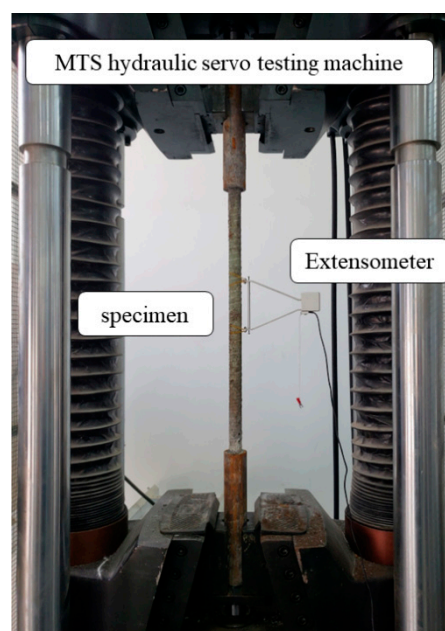


Figure 2. MTS100 test equipment.

4.3. Experiment Procedure

4.3.1. Preparation of Test Pieces

Epoxy adhesive was used to join steel pipes and GFRP bars, forming three distinct types of test specimens with diameters of 10, 12, and 25 mm and corresponding lengths of 840, 920, and 1440 mm. The ends of these specimens were encased in steel pipes, each 220 mm in length, and then filled with epoxy resin. This assembly underwent a specific curing process before the materials were subjected to testing, ensuring a robust preparation phase [33].

The reliability of adhesive application makes it challenging to ensure quality, leading to a high risk of slip damage, particularly in specimens with a 10 mm diameter. To enhance the bonding effectiveness, the steel pipe was longitudinally divided into sections. Subsequently, epoxy resin was applied to adhere these bisected steel pipe sections to the GFRP bars, a modification aimed at improving the overall integrity and bonding strength of the assembly.

4.3.2. Tensile Test

The test adopts the displacement loading method, and the loading strain rate is about $5 \times 10^{-5} \text{ s}^{-1}$. The mechanical properties such as ultimate tensile strength, elastic modulus, and ultimate elongation were determined through the recorded data.

5. Results and Discussion

5.1. Ultimate Tensile Strength

The ultimate tensile strength of GFRP bars with different diameters obtained from the test is shown in Table 1.

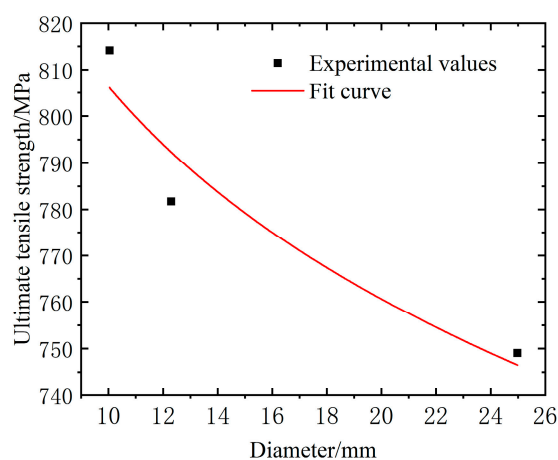
Regression analysis was carried out on the relationship between the diameter and the ultimate tensile strength, and the fitting formula of the ultimate tensile strength f_{Dtu} of the specimen considering the influence of the diameter was obtained. The change law is in the form of a power function. The fitting image is shown in Figure 3:

$$f_{Dtu} = 978.64D^{-0.084} \quad (6)$$

Table 1. Ultimate strength of GFRP bars with different diameters.

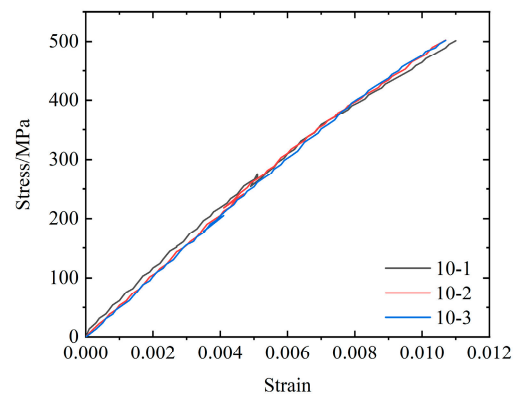
D_0/mm	D/mm	A/mm^2	F/kN	σ/MPa	$\text{Avg.}/\text{MPa}$	SD	COV	E/GPa
10	10.04	79.17	65.17	823.17	814.16	13.48	0.0166	50.5
			63.23	798.67				
			64.97	820.65				
12	12.3	118.82	93.49	786.80	781.72	4.79	0.0061	51.95
			92.36	777.29				
			92.81	781.08				
25	24.98	490.09	373.34	761.78	749.04	12.35	0.0165	54.43
			366.69	748.21				
			361.26	737.13				

Note: In the table, D_0 is the size provided by the merchant, D is the measured size, F is the ultimate tensile bearing capacity, σ is the ultimate tensile strength, Avg. is the mean value of stress, SD is the standard deviation of stress, and COV is the coefficient of variation.

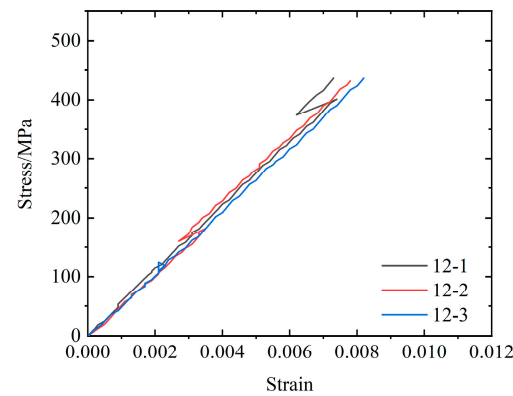
**Figure 3.** Power function fitting of ultimate tensile strength and diameter of specimen (using Formula (6)).

5.2. Stress–Strain Relationship

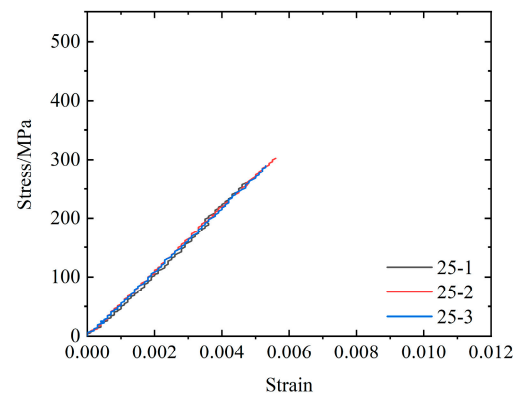
According to the measured results, the test stress–strain curves of GFRP tendons were drawn. The stress–strain curves of GFRP tendons with diameters of 10, 12, and 25 mm are shown in Figure 4. The curves do not display the entire stress–strain relationship up to failure due to the removal of the extensometer prior to specimen failure, which is a common practice to avoid damaging the device [34]. The test results show that the tensile elastic modulus increases with respect to the diameter while the elongation capacity diminishes as the bar becomes larger. For the 10 mm bar, the curves are closely packed, showing a consistent response among the samples tested with an initial modulus similar for all three specimens. Conversely, the 12 mm diameter displays greater divergence than the 10 mm. This could indicate a more pronounced effect of the larger diameter on stress distribution. The nonlinear portions of the curve are more obvious. For the 25 mm bar, the stress–strain curves show less strain at similar stress levels compared to the other bars, suggesting a higher modulus of elasticity. This could be expected as larger diameters generally provide more resistance to deformation. The curves are relatively straight, suggesting good accuracy and acceptable measurement precision.



(a)



(b)



(c)

Figure 4. Stress–strain curves of GFRP tendons with different diameters. (a) Stress–strain curve of 10 mm diameter GFRP tendon. (b) Stress–strain curve of 12 mm diameter GFRP tendon. (c) Stress–strain curve of 25 mm diameter GFRP tendon.

The relationship between the tensile elastic modulus, yield strain, ultimate elongation, and diameter was assessed using regression analysis. For each of the parameters, its relations with the diameter were established and the following formulas are proposed:

$$E_{D0} = 58.83D - 0.20 \quad (7)$$

$$E_{D1} = 52.88D \quad (8)$$

$$\varepsilon_{Dy} = 0.004445D^{0.1846} \quad (9)$$

$$\delta_D = 3.15D - 0.29 \quad (10)$$

In the formula, E_D is tensile modulus of elasticity, ε_{Dy} the strain, δ_D the ultimate elongation, and D the diameter of GFRP tendon specimen.

5.3. Failure Mode

There are two failure modes of the specimen: the fracture of the specimen (which is an effective failure mode) and the slippage out of the anchorage due to an insufficient bond strength between the anchorage at the end of the specimen and the specimen itself.

During the testing phase, as the load on the specimen increases between 20% and 30% of its maximum capacity, audible signs of damage start to emerge, characterized by a series of sharp, distinct sounds indicating initial damage. As the load further escalates to the 60–70% threshold of the ultimate load, these audible indicators intensify, becoming more frequent and pronounced until they culminate in a significant cracking noise, signaling the specimen's abrupt and catastrophic failure.

Remarkably, at approximately half of the specimen's maximum load capacity, visual manifestation of degradation becomes apparent in the form of fine, white cracks spreading across the surface. This stage marks a critical juncture in the specimen's integrity, highlighting the onset of structural weakening.

Failure modes of the specimens are broadly categorized into two distinct types. The first and more prevalent type involves widespread cracking, rendering the specimen incapable of supporting any further load. The second, less common type, is characterized by a complete break at a specific section of the specimen, leading to an immediate loss of load-bearing capacity. Both failure modes are indicative of a brittle fracture mechanism, obviously demonstrated in the experimental findings. This brittle nature of failure is illustrated in Figure 5, serving as a visual confirmation of the specimen's inability to deform plastically before breaking, thus underscoring the critical observations made during the loading process.



Figure 5. Specimen failure mode.

6. Analysis of Size Effect of GFRP Tendon Strength

GFRP tendon is a kind of composite material, and its ultimate tensile strength is affected by factors such as process and environment, and there are inevitably many defects (micro cracks, nicks, etc.) on the surface and inside of the material. Moreover, the ultimate tensile strength of the material often depends on the weakest link in these randomly distributed defects. As the diameter of the specimen increases, the number of randomly distributed defects increases, and the corresponding strength decreases. This material behavior is in good agreement with the assumptions of the weakest chain theory. Assuming

that the strength distribution of GFRP tendons conforms to the Weibull distribution law, the size effect analysis of GFRP tendon strength can be carried out.

6.1. Ultimate Tensile Strength

In the experiment, the GFRP tendon specimens were used with diameters of 10, 12, and 25 mm, featuring effective lengths of 400, 480, and 1000 mm, respectively. Each length was precisely 40 times its corresponding diameter. The volume of the 10 mm diameter specimen reached $31,668 \text{ mm}^3$, presenting an ultimate tensile strength of 814.16 MPa. For the 12 mm diameter specimen, the volume expanded to $57,033.6 \text{ mm}^3$, alongside an ultimate tensile strength of 781.72 MPa. The largest, a 25 mm diameter specimen, had a significant volume of $490,090 \text{ mm}^3$, with its ultimate tensile strength recorded at 749.04 MPa. These observations are graphically represented in a logarithmic plot concerning volume against ultimate tensile strength, as displayed in Figure 6. An equation was derived to fit the plotted line, encapsulating the relationship between the variables under study, which underscores the critical insights obtained from the experimental data.

$$\ln \sigma = 6.9773 - 0.0276 \ln V \quad (11)$$

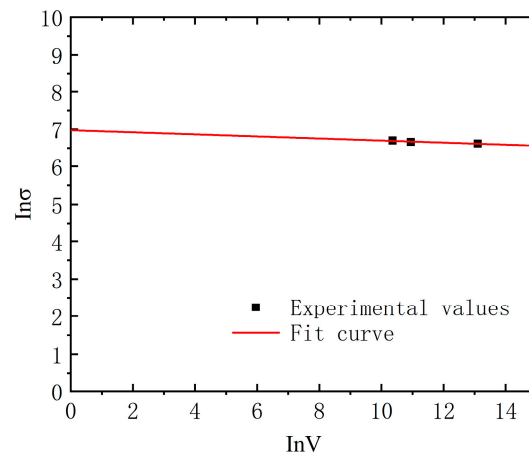


Figure 6. Linear fitting of logarithmic value of ultimate tensile strength and logarithmic volume according to Formula (11), $\sigma_0 = 1072.02 \text{ MPa}$, $m = 36.2319$.

6.2. Prediction of GFRP Tendon Strength

Assuming that the length of the GFRP tendon specimen is 40 times its diameter, and substituting m and volume into Equation (5), the ultimate tensile strength can be predicted.

The ultimate tensile strength of a 16 mm diameter GFRP tendon is as follows:

$$\sigma_2 = \left(\frac{V_1}{V_2}\right)^{\frac{1}{m}} \sigma_1 = \left(\frac{31668}{128680}\right)^{0.0276} \times 814.16 = 783.26 \text{ MPa} \quad (12)$$

The ultimate tensile strength of GFRP bars with a diameter of 22 mm is as follows:

$$\sigma_2 = \left(\frac{V_1}{V_2}\right)^{\frac{1}{m}} \sigma_1 = \left(\frac{31668}{334516}\right)^{0.0276} \times 814.16 = 762.87 \text{ MPa} \quad (13)$$

It can be seen that the weakest link theory analysis of GFRP based on the strength conforming to the Weibull distribution law Rib strength size effect is feasible.

6.3. Determination of the GFRP Tendon Strength's Standard Value

Based on the weakest link theory, the parameters σ_0 and m are obtained from the test data, and the probability of failure of the specimen at a certain stress level can be calculated.

By substituting the calculated values of σ_0 and m into Equation (3) we obtain the following equation:

$$Fv(\sigma) = 1 - \exp \left[-V \left(\frac{\sigma}{1072.02} \right)^{36.2319} \right] \quad (14)$$

The failure probabilities of the three diameter specimens in the current test are 77.3%, 65.8%, and 67.4%, respectively.

If the strength guarantee rate is 95%, the standard tensile strength values of GFRP tendons with diameters of 10, 12, and 25 mm are calculated according to Formula (14) to be 541.42 MPa, 519.84 MPa, and 498.11 MPa, respectively, which is equivalent to 70% of the ultimate tensile strength.

6.4. Discussion on Reasonable Length of Test Piece

According to the analysis of the weakest chain theory, the influencing factor of the size effect of GFRP tendon is mainly the effective area volume of the specimen, which not only includes the diameter of the GFRP tendon but also the length of the specimen. In order to guarantee the tensile strength rate of the GFRP bars used in the design to be at the same level, it is necessary to unify the selection standard of the length of the test piece. It is recommended that the length of the specimen be a multiple of the diameter of the GFRP tendon, so that the influence factor of the size effect of the GFRP tendon is normalized to the diameter.

According to the test level of this paper, the ultimate tensile strength of different multiples of the diameter (10 mm) is calculated by using Formula (5). The results are shown in Table 2.

Table 2. Ultimate tensile strength of GFRP bars with different lengths.

Effective Length of Test Piece	10D	20D	30D	40D	50D	60D	70D	80D
ultimate tensile strength/MPa	845.92	829.89	820.65	814.16	809.16	805.10	801.68	798.73

It can be seen from Table 2 that the strength decreases with the increase in length, and the difference is also smaller. Compared with the strength of 10D when the length is 20D, the strength difference reaches 1.8%. Compared with the strength of 40D, 30D, and 50D, the strength difference reaches 0.71% and 0.62%, respectively. When the length is not less than 30D, if the difference in the length of the specimens is not large, it will have little effect on the measured strength. In order to conform to the actual situation, the effective length of the test piece should be designed as large as possible, and the feasibility of the test should also be considered. Limited to the space of the equipment, the length of the specimen should not be too large. The length of the specimen consists of the effective length and the anchorage length at both ends. The total length of anchorage at both ends is about 35D. It is recommended that the effective length of the specimen be 30D to 40D.

7. Conclusions

In this paper, GFRP tendons with different diameters were used to study the size effect of the tensile mechanical properties through experiments, and the following conclusions were obtained:

- (1) The mechanical properties of GFRP tendons have an obvious size effect. As the diameter increases, the tensile modulus increases while the strain decreases.
- (2) The correlation formulas of ultimate tensile strength, stress–strain relationship, and diameter of GFRP tendons were obtained through experiments. The experimental results show that the logarithm of stress and volume has a linear relationship, which indicates that it is feasible to analyze the size effect based on the weakest chain theory that the strength of GFRP tendons conforms to the Weibull distribution law.

(3) Based on the weakest chain theory, the strength of different GFRP tendons can be predicted. The standard value of the tensile strength is determined, and the parameters σ_0 and m are obtained from the experimental data. Hence, it is possible to calculate the probability of specimen failure at a certain stress level.

(4) Based on the weakest chain theory that the strength of GFRP tendons conforms to the Weibull distribution law, a linear fitting relationship between the logarithm of ultimate tensile strength and the logarithm of volume is proposed. Therefore, the main factor affecting the size effect of GFRP tendons is the volume of the effective area of the specimen.

(5) As the length increases, the strength decreases, and the difference is smaller. When the length is not less than $30D$, the difference in the length of the test piece is not large, and the measured strength has little effect. In order to conform to the actual situation, it is recommended to unify the effective length selection standard of GFRP tendon specimens, which ranges from 30 to 40 times the diameter of the specimen.

As a new type of composite material, GFRP tendons are discussed in this paper on the size effect of the scale range of laboratory specimens. When GFRP tendons are applied to large structural members, the size effect of material mechanical properties should attract attention. On the other hand, we acknowledge that the experimental investigation was conducted under controlled laboratory conditions, which may not fully represent the complex and diverse conditions encountered in real-world applications. Furthermore, this study focuses solely on GFRP bar tensile strength, while other important mechanical properties such as flexural and shear strength have not been examined. It is thus important to conduct further research to address these aspects and enhance the applicability of the analysis.

Author Contributions: Data curation, J.L. and S.G.; Formal analysis, J.L. and T.A.K.; Investigation, H.L., N.S. and S.G.; Methodology, Y.Z.; Project administration, T.T.; Supervision, H.L. and T.A.K.; Visualization, S.G.; Writing—original draft, J.L.; Writing—review and editing, T.A.K., T.T., H.L., N.S. and Y.Z. All authors have read and agreed to the published version of the manuscript.

Funding: This research received no external funding.

Data Availability Statement: Data are contained within the article.

Conflicts of Interest: Authors Hongbo Liu and Nianjiu Su were employed by the company Poly Changda Engineering Co., Ltd. Author Yaoyu Zhu was employed by the company CCC Highway Bridges National Engineering Research Center Co., Ltd. The remaining authors declare that the research was conducted in the absence of any commercial or financial relationships that could be construed as a potential conflict of interest.

References

- Li, G.; Huang, Z.; Zhang, D.; Wang, S. Field Test on Load-Bearing Character of Glass Fiber Reinforced Polymer Bolt. *Chin. J. Rock Mech. Eng.* **2006**, *25*, 2240. (In Chinese)
- Xue, W.; Kang, Q. Application of Fiber Reinforced Plastic Reinforcement in Concrete Structure. *Ind. Archit.* **1999**, *29*, 20–22–29. (In Chinese)
- Zhao, G. Development and Application of Concrete and Its Reinforcement Materials. *J. Build. Mater.* **2000**, *3*, 8–13. (In Chinese)
- Carvelli, V.; Fava, G.; Pisani, M.A. Anchor System for Tension Testing of Large Diameter GFRP Bars. *J. Compos. Constr.* **2009**, *13*, 344–349. [[CrossRef](#)]
- D’antino, T.; Pisani, M.A.; Poggi, C. Effect of the Environment on the Performance of GFRP Reinforcing Bars. *Compos. Part B Eng.* **2018**, *141B*, 123–136. [[CrossRef](#)]
- ACI Committee. ACI 440 Recommended Test Methods for FRP Rods and Sheets. *Second. J.* **2002**.
- Li, G.; Wu, J.; Ge, W. Effect of Loading Rate and Chemical Corrosion on the Mechanical Properties of Large Diameter Glass/Basalt-Glass Frp Bars. *Constr. Build. Mater.* **2015**, *93*, 1059–1066. [[CrossRef](#)]
- Hamad, R.J.A.; Johari, M.A.M.; Haddad, R.H. Mechanical Properties and Bond Characteristics of Different Fiber Reinforced Polymer Rebars at Elevated Temperatures. *Constr. Build. Mater.* **2017**, *142*, 521–535. [[CrossRef](#)]
- Najafabadi, E.P.; Oskouei, A.V.; Khaneghahi, M.H.; Shoaee, P.; Ozbakkaloglu, T. The Tensile Performance of FRP Bars Embedded in Concrete under Elevated Temperatures. *Constr. Build. Mater.* **2019**, *211*, 1138–1152. [[CrossRef](#)]
- Devon, E.; Habib, T.; Azam, N. Residual Tensile Strength and Bond Properties of Gfrp Bars after Exposure to Elevated Temperatures. *Materials* **2018**, *11*, 346. [[CrossRef](#)]

11. Ashrafi, H.; Bazli, M.; Najafabadi, E.P.; Oskouei, A.V. The Effect of Mechanical and Thermal Properties of FRP Bars on Their Tensile Performance under Elevated Temperatures. *Constr. Build. Mater.* **2017**, *157*, 1001–1010. [[CrossRef](#)]
12. Rifai, M.A.; El-Hassan, H.; El-Maaddawy, T.; Abed, F. Durability of Basalt FRP Reinforcing Bars in Alkaline Solution and Moist Concrete Environments. *Constr. Build. Mater.* **2020**, *243*, 118258. [[CrossRef](#)]
13. Xie, Q.; Wang, X.; Wu, G.; Dong, Z. Degradation of Basalt FRP Bars in Alkaline Environment. *Sci. Eng. Compos. Mater.* **2015**, *22*, 649–657.
14. Ahmed, A.; Guo, S.; Zhang, Z.; Shi, C.; Zhu, D. A Review on Durability of Fiber Reinforced Polymer (FRP) Bars Reinforced Seawater Sea Sand Concrete. *Constr. Build. Mater.* **2020**, *256*, 119484. [[CrossRef](#)]
15. Hu, X.; Guan, J.; Wang, Y.; Keating, A.; Yang, S. Comparison of Boundary and Size Effect Models Based on New Developments. *Eng. Fract. Mech.* **2017**, *175*, 146–167. [[CrossRef](#)]
16. Vu, C.C.; Weiss, J.; Ple, O.; Amitrano, D.; Vandembroucq, D. Revisiting Statistical Size Effects on Compressive Failure of Heterogeneous Materials, with a Special Focus on Concrete. *J. Mech. Phys. Solids* **2018**, *121*, 47–70. [[CrossRef](#)]
17. Li, Y.; Zheng, Z.; Jin, X. Analysis and Application of Bazant Size Effect Law. *China Build. Sci. Core Period.* **2003**, *2*, 35–36. (In Chinese)
18. Liu, H.; Yu, X.; Li, G. Experimental Study on Tensile Mechanical Properties of Glass Fiber Reinforced Plastic Rebar. *Chin. J. Rock Mech. Eng.* **2005**, *24*, 121–125. (In Chinese)
19. Zheng, L.; Luo, Y.; Huang, P. Experimental and Theoretical Research on the Fracture Strength of Fiberglass Reinforcement. *J. Mech. Strength* **2004**, 104–106. (In Chinese)
20. ACI Committee. ACI 440.1 R-03: Guide for the Design and Construction of Concrete Reinforced with Frp Bars. *Second. J.* **2001**. [[CrossRef](#)]
21. Nassiraei, H.; Rezadoost, P. Static Capacity of Tubular X-Joints Reinforced with Fiber Reinforced Polymer Subjected to Compressive Load. *Eng. Struct.* **2021**, *236*, 112041. [[CrossRef](#)]
22. Lee, J.Y.; Lim, A.R.; Kim, J.; Kim, J. Bond Behaviour of GFRP Bars in High-Strength Concrete: Bar Diameter Effect. *Mag. Concr. Res.* **2017**, *69*, 541–554. [[CrossRef](#)]
23. Sun, L.; Wang, C.; Zhang, C.; Yang, Z.; Li, C.; Qiao, P. Experimental Investigation on the Bond Performance of Sea Sand Coral Concrete with Frp Bar Reinforcement for Marine Environments. *Adv. Struct. Eng.* **2023**, *26*, 533–546. [[CrossRef](#)]
24. Zhang, B.; Zhu, H.; Cao, R.; Ding, J.; Chen, X. Feasibility of Using Geopolymers to Investigate the Bond Behavior of Frp Bars in Seawater Sea-Sand Concrete. *Constr. Build. Mater.* **2021**, *282*, 122636. [[CrossRef](#)]
25. Demiral, M.; Kadioglu, F.; Silberschmidt, V.V. Size Effect in Flexural Behaviour of Unidirectional GFRP Composites. *J. Mech. Sci. Technol.* **2020**, *34*, 5053–5061. [[CrossRef](#)]
26. Alajarmeh, O.; Manalo, A.; Benmokrane, B.; Vijay, P.; Ferdous, W.; Mendis, P. Novel Testing and Characterization of Gfrp Bars in Compression. *Constr. Build. Mater.* **2019**, *225*, 1112–1126. [[CrossRef](#)]
27. Zhou, J.; Du, Q.Q.; Chen, L.; Ma, X.H. Experimental Study on Size Effect in Tensile Mechanical Properties of Gfrp Rebar. *J. Hohai Univ.* **2008**, *36*, 242–246.
28. Abdelkarim, O.I.; Ahmed, E.A.; Mohamed, H.M.; Benmokrane, B. Flexural Strength and Serviceability Evaluation of Concrete Beams Reinforced with Deformed GFRP Bars. *Eng. Struct.* **2019**, *186*, 282–296. [[CrossRef](#)]
29. Zinkaah, O.H.; Ashour, A. Load Capacity Predictions of Continuous Concrete Deep Beams Reinforced with GFRP Bars. *Structures* **2019**, *19*, 449–462. [[CrossRef](#)]
30. Sutherland, L.S.; Shenoi, R.A.; Lewis, S.M. Size and Scale Effects in Composites: I. Literature Review. *Compos. Sci. Technol.* **1999**, *59*, 209–220. [[CrossRef](#)]
31. Bazant, Z.P.; Chen, E.P. Scaling of Structural Failure. *Appl. Mech. Rev.* **1997**, *50*, 593–627. [[CrossRef](#)]
32. Wisnom, M.R. Size Effects in the Testing of Fibre-Composite Materials. *Compos. Sci. Technol.* **1999**, *59*, 1937–1957. [[CrossRef](#)]
33. Kai, Z.; Qing, D.; Yun, L.; Xue, C. Experimental Study of Glass Fiber Reinforced Polymer Bar Joint. *China Acad. J. Electron. Publ. House* **2006**, *5*, 24–27. (In Chinese)
34. Cendón, D.; Atienza, J.M.; Elices Calafat, M. Strain Localisation During a Tensile Test of Metallic Plates: Experimental and Numerical Results. *Key Eng. Mater.* **2010**, *417*, 569–572. [[CrossRef](#)]

Disclaimer/Publisher’s Note: The statements, opinions and data contained in all publications are solely those of the individual author(s) and contributor(s) and not of MDPI and/or the editor(s). MDPI and/or the editor(s) disclaim responsibility for any injury to people or property resulting from any ideas, methods, instructions or products referred to in the content.